allowing only the next nearest position (i.e., shifts of ±2) did not reproduce the measured diffuse scattering as well. The disorder shown schematically in Fig. 2B reflects the approximate frequency found for the different shifts. Further fine-tuning revealed that there is no correlation between the positions of the 12-rings in the two halves of the unit cell along the long **c** axis.

The disordered structure described above is fully consistent with the HRTEM images (*5*), which show predominantly single-step displacements from layer to layer. The fact that none of the images shows larger 12-ring openings is also consistent with the lack of open 12-ring channels. The ladderlike regions between the ZSM-11 regions are those in which 12-rings are partially blocked by 10-rings (Fig. 2). Although the basic channel system of SSZ-57 is the same as that of ZSM-11, there are additional bulges in the channels where the 12-rings occur (Fig. 4). That is, SSZ-57 has a 3D 10-ring channel system with a dilute population of larger isolated cavities. These loosely ordered cavities must be the reason for the different catalytic properties observed for this material.

It has been shown for the zeolites SSZ-25 (**MWW**) and SSZ-35 (**STF**), which have 10-ring apertures leading to larger cavities, that their catalytic selectivities reflect the presence of these less-restricted regions (*24*). The situation with SSZ-57 is different in that the larger cavities are more highly dispersed in the 10-ring channel system. In the idealized structure (Fig. 1A), which does not actually exist as an extended structure, there would be just single 12-ring channels embedded in the 10-ring ZSM-11 framework. Only as a result of the disorder are the 12-ring pockets distributed throughout the structure, thereby providing SSZ-57 with its unique properties. The 12-ring pockets provide space for larger intermediates (e.g., for bimolecular transition states) in a catalytic reaction and/or faster diffusion, whereas the 10-ring channel system preserves the shape-selective sorption and desorption properties of a classical pentasil framework structure. This could be particularly valuable in forming products for fine chemicals, where modification of the substituents of single rings, either by acid-catalyzed or partial oxidation reactions, is often required.

The crystallization mechanism of SSZ-57 remains to be clarified, but the synthesis is quite reproducible. This structure could be viewed as a first step along the way to a hierarchical material (microporous system with mesopores to facilitate diffusion) with well-defined mesopores. Other attempts in this direction have involved carving mesoporosity into zeolite crystals, cotemplating the formation of both types of pores (*25*), and producing a material with arrested crystallization (*26*). SSZ-57 offers a fourth option.

References and Notes

1. S. Elomari, U.S. Patent 6,544,495 (2003).
2. Framework type codes for all zeolites mentioned in the text are given in parentheses.
3. A. W. Burton *et al.*, *Stud. Surf. Sci. Catal.* **170**, 690 (2007).
4. S. I. Zones *et al.*, *J. Catal.* **250**, 41 (2007).
5. S. I. Zones *et al.*, *Solid State Sci.* **13**, 706 (2011).
6. An *n*-ring is a ring of *n* Si atoms alternating with *n* O atoms that defines the dimensions of a pore opening in a zeolite framework structure. A 10-ring is usually referred to as a medium, and a 12-ring as a large, pore opening.
7. S. Elomari, U.S. Patent 6,616,830 (2003).
8. C. Baerlocher, L. B. McCusker, D. H. Olson, *Atlas of Zeolite Framework Types* (Elsevier, Amsterdam, 2007).
9. H. Gies, H. van Koningsveld, Catalog of Disorder in Zeolite Frameworks, www.iza-structure.org/databases.
10. C. Broennimann *et al.*, *J. Synchrotron Radiat.* **13**, 120 (2006).
11. G. T. Kokotailo, P. Chu, S. L. Lawton, W. M. Meier, *Nature* **275**, 119 (1978).
12. F. Gramm *et al.*, *Nature* **444**, 79 (2006).
13. C. Baerlocher *et al.*, *Science* **315**, 1113 (2007).
14. Materials and methods are available as supporting material on *Science* Online.
15. G. M. Sheldrick, *Acta Crystallogr. A* **64**, 112 (2008).
16. S. van Smaalen, *Incommensurate Crystallography* (Oxford Univ. Press, Oxford, 2007).
17. G. Oszlányi, A. Sütö, *Acta Crystallogr. A* **60**, 134 (2004).
18. G. Oszlányi, A. Sütö, *Acta Crystallogr. A* **64**, 123 (2008).
19. L. Palatinus, *Acta Crystallogr. A* **60**, 604 (2004).
20. L. Palatinus, G. Chapuis, *J. Appl. Cryst.* **40**, 786 (2007).
21. L. Palatinus, A. van der Lee, *J. Appl. Cryst.* **41**, 975 (2008).
22. V. Petricek, M. Dusek, L. Palatinus, Jana2006 (Institute of Physics, Prague, Czech Republic, 2006).
23. C. Baerlocher, A. Hepp, W. M. Meier, DLS-76, Distance least squares refinement program (Institut für Kristallographie, ETH Zürich, Switzerland, 1977).
24. J. R. Carpenter, S. Yeh, S. I. Zones, M. E. Davis, *J. Catal.* **269**, 64 (2010).
25. J.-B. Koo *et al.*, *J. Catal.* **276**, 327 (2010).
26. J. Kim, W. Park, R. Ryoo, *ACS Catal* **1**, 337 (2011).
27. S. Brenner, L. B. McCusker, C. Baerlocher, *J. Appl. Cryst.* **30**, 1167 (1997).

Acknowledgments: We thank S. Elomari for synthesizing the SSZ-57 sample. Crystallographic experiments were conducted at the X06SA beamline at the Swiss Light Source, Paul Scherrer Institute, Villigen, Switzerland. We thank the staff there for assistance with the data collection. This work was funded in part by the Swiss National Science Foundation. Additional information on the indexing, the structure solution, the model construction and the Monte Carlo simulations is available in the supporting online material.

Supporting Online Material

www.sciencemag.org/cgi/content/full/333/6046/1134/DC1
Materials and Methods
SOM Text
Figs. S1 to S4
Tables S1 and S2
References

25 April 2011; accepted 25 July 2011
10.1126/science.1207466

optix Drives the Repeated Convergent Evolution of Butterfly Wing Pattern Mimicry

Robert D. Reed,[1*†] Riccardo Papa,[1,2*†] Arnaud Martin,[1] Heather M. Hines,[3] Brian A. Counterman,[4] Carolina Pardo-Diaz,[5] Chris D. Jiggins,[5] Nicola L. Chamberlain,[6] Marcus R. Kronforst,[6] Rui Chen,[7] Georg Halder,[8] H. Frederik Nijhout,[9] W. Owen McMillan[10,3]

Mimicry—whereby warning signals in different species evolve to look similar—has long served as a paradigm of convergent evolution. Little is known, however, about the genes that underlie the evolution of mimetic phenotypes or to what extent the same or different genes drive such convergence. Here, we characterize one of the major genes responsible for mimetic wing pattern evolution in *Heliconius* butterflies. Mapping, gene expression, and population genetic work all identify a single gene, *optix*, that controls extreme red wing pattern variation across multiple species of *Heliconius*. Our results show that the cis-regulatory evolution of a single transcription factor can repeatedly drive the convergent evolution of complex color patterns in distantly related species, thus blurring the distinction between convergence and homology.

Some of the most dramatic examples of natural selection involve Müllerian mimicry—a phenomenon in which two or more species share predator avoidance signals. This type of mimicry is one of the main forces driving the evolution of warning coloration in *Heliconius* (*1*), a neotropical butterfly genus of ~40 species famous for its extensive intraspecific wing pattern variation. The two best-studied *Heliconius* species are the comimics *Heliconius erato* and *Heliconius melpomene* (Fig. 1); each has more than 25 named geographic races, most of which mimic co-occurring *Heliconius* species, other unrelated butterflies, and day-flying moths. Mimetic wing pattern radiations like those seen in *H. erato*

[1]Department of Ecology and Evolutionary Biology, University of California, Irvine, CA 92697, USA. [2]Department of Biology and Center for Applied Tropical Ecology and Conservation, University of Puerto Rico, Rio Piedras, Puerto Rico. [3]Department of Genetics, North Carolina State University, Raleigh, NC 27695, USA. [4]Department of Biological Sciences, Mississippi State University, Mississippi State, MS 39762, USA. [5]Department of Zoology, University of Cambridge, Cambridge CB2 3EJ, UK. [6]FAS Center for Systems Biology, Harvard University, Cambridge, MA 02138, USA. [7]Baylor Human Genome Sequencing Center, Houston, TX 77030, USA. [8]Department of Biochemistry and Molecular Biology, M.D. Anderson Cancer Center, University of Texas, Houston, TX 77030, USA. [9]Department of Biology, Duke University, Durham, NC 22708, USA. [10]Smithsonian Tropical Research Institute, Panama City, Panama.

*These authors contributed equally to this work.
†To whom correspondence should be addressed. E-mail: rreed@uci.edu (R.D.R.); rpapa.lab@gmail.com (R.P.)

and *H. melpomene* have resulted in the evolution of hundreds of wing pattern races within the genus (*2*). Despite increasing evidence that the same genomic regions contribute to wing pattern variation in different *Heliconius* species, the specific genes that underlie the repeated convergent evolution of wing patterns have remained unknown (*3*).

Three genomic regions control most wing pattern variation in *Heliconius*—in both comimetic species like *H. erato* and *H. melpomene* and also in highly dissimilar species such as *Heliconius numata* and *Heliconius cydno* (*3*). The region that controls the major red color patterns (the hindwing rays, forewing band, and basal forewing patch) maps to a 380-kb genomic interval corresponding to the *D* locus in *H. erato* and *H. melpomene* (*4*, *5*) and the *G* locus in *H. cydno* (*6*). To pinpoint transcription units in this interval involved in wing pattern variation we screened for differential color pattern–related RNA transcription across the entire region. We examined two *H. erato* forewing phenotypes: one with a red midwing band, and one with a yellow midwing band and a red basal patch (Fig. 2A). For both phenotypes, we compared transcription in basal, midwing, and apical wing sections from five different developmental stages (Fig. 2A). This strategy allowed us to perform separate comparisons of each distinct red color pattern element, while also including comparisons between invariant apical forewing tips to control for population-associated expression differences unrelated to phenotype. A global analysis of all stages and tissue sections from the two phenotypes identified a single major cluster of red color pattern–associated probes at the position of *optix* (Fig. 2A), an intronless homeobox transcription factor gene with an 801–base pair coding region. Further analysis of the data revealed that this pattern-specific differential expression of *optix* begins between 12 and 60 hours after pupation and persists throughout pupal development (fig. S1). No other genes in the map interval besides *optix* were consistently expressed in association with color pattern variation.

The finding that *optix* is differentially expressed in association with red color patterns in two *H. erato* phenotypes raised the question of whether *optix* expression is also associated with red patterns in other *H. erato* races and other *Heliconius* species. We thus examined in situ spatial expression patterns of *optix* mRNA in 72-hour pupal forewings and hindwings across a diversity of phenotypes and species. Across three geographic races of *H. erato*, three races of *H. melpomene*, and one race of *H. cydno*, we found that all red wing patterns, including red hindwing rays in both *H. erato* and *H. melpomene*, were perfectly prefigured by *optix* expression (Fig. 2, B and C). *optix* also prefigured forewing bands in *H. melpomene plesseni* that consist of both red and white scales (Fig. 2B), consistent with the activity of an unlinked modifier locus that modulates the amount of red in forewing bands (*7*). Overall, *optix* expression predicted color pattern shapes with such precision that it was possible to identify samples to species and race by *optix* expression alone.

The concurrence of mapping and expression data led us to hypothesize that *optix* is the major gene that controls red color pattern variation in *H. erato*, *H. melpomene*, and *H. cydno*. To test this, we examined *optix* genotype-by-phenotype associations in hybrid zones where there is natural variation for *optix*-associated red color patterns (Fig. 3). These hybrid zones consist of populations that represent thousands of generations of recombination between wing pattern types; therefore, DNA sequence associations are due to linkage with functional variation and not other phenomena like population structure (*8*, *9*). In a Peruvian *H. erato* hybrid zone where linkage disequilibrium is reported to decay to background levels within 1 kb (*8*), we examined DNA sequence variation in a series of red color pattern interval genes from 73 individuals (Fig. 3B). *optix* showed by far the strongest association, with 13 of 30 variable nucleotides having significant associations of $P < 1 \times 10^{-15}$, with the strongest being $P < 1 \times 10^{-32}$ (Fig. 3B and table S2). Similarly, we sampled 62 individuals from the parallel Peruvian *H. melpomene* hybrid zone and found that *optix* showed the most significant associations of any sampled marker, with 5 of 29 variable nucleotides having significant associations of $P < 1 \times 10^{-10}$, with the strongest being $P < 1 \times 10^{-32}$ (Fig. 3C and table S3). In *H. melpomene*, a cluster of genes (*slu7*, *kinesin*, *GPCR*) ~150 kb away from *optix* showed a total of six nucleotide associations with $P < 1 \times 10^{-10}$ (Fig. 3C), though none of these genes displayed color pattern–related spatial expression and they showed only marginal associations in *H. erato*. This broad spread of associated nucleotides in *H. melpomene* is consistent with the observation that linkage disequilibrium in this hybrid zone can extend 100 kb or more at wing pattern–associated sites (*9*). Lastly, we assessed *optix* genotype-by-phenotype associations in 32 individuals collected from the Costa Rican *H. cydno*/*H. pachinus* hybrid zone wherein, as with *H. erato*, highly significant associations are only expected within 1 kb of functional variation (*6*). Of all the sampled genes, *optix* had the most significant association with a nucleotide that showed $P < 1 \times$

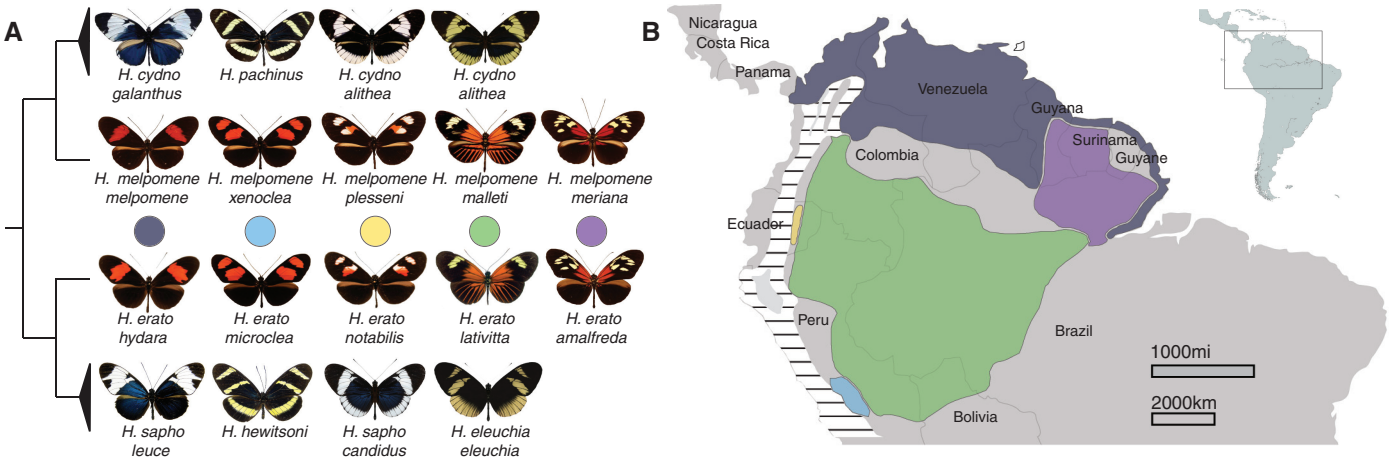

Fig. 1. Mimicry rings show convergent and divergent evolution within *Heliconius*. (**A**) Comimetic *Heliconius* species are typically distantly related as shown in this phylogenetic tree of selected *Heliconius* species. Illustrated are two major mimicry groups: the blue mimics represented by the *H. cydno*/*H. pachinus* complex and the *H. sapho*/*H. hewitsonii*/*H. eleuchia* complex, and the red/yellow mimics represented by *H. erato* and *H. melpomene*. In addition to local convergence, wing patterns often vary markedly across the geographic range of a species to match local mimicry rings. For *H. cydno*, we show three of more than a dozen color pattern races. For the red/yellow mimicry ring, we show five of more than 25 different geographic races of *H. erato* and *H. melpomene*. (**B**) Simplified geographic distribution of the *H. erato* and *H. melpomene* color pattern forms shown in (A), as color-coded by the dots. The entire range of *H. erato* and *H. melpomene* is much larger (gray shaded region).

10^{-12} (Fig. 3E and table S4). Together, these three independent population genetic analyses all pinpoint *optix* as the major gene that controls red color pattern variation.

Because *optix* alleles from different geographic races of *Heliconius* show clear differences in spatial expression patterns (Fig. 2B), it follows that there are cis-regulatory differences between alleles. To rule out allelic variation in optix protein amino acid sequences, we sequenced the entire coding region of *optix* from *H. erato emma*, *H. erato favorinus*, *H. erato petiverana*, *H. melpomene rosina*, *H. melpomene melpomene*, *H. pachinus*, and *H. cydno galanthus*. All variation that we observed was synonymous, meaning that despite 12 to 25 million years of evolution (*10*) the *optix* amino acid sequence has remained invariable. This was true between highly divergent races of the same species (within *H. erato*), between divergent phenotypes of closely related species (*H. cydno* versus *H. melpomene*), and between convergent phenotypes of distantly related species (*H. erato* versus *H. melpomene*). Thus, when considered in the context of the mapping work, we deduce that the functional variation between *optix* alleles is cis-regulatory.

To make an initial assessment of whether *optix* is associated with color pattern determination in non-*Heliconius* butterflies and moths, we examined in situ *optix* mRNA expression in 72-hour pupal wings of the nymphalid butterflies *Vanessa cardui* (Fig. 2D) and *Agraulis vanillae* (fig. S2), and the pyralid moth *Ephestia kuehniella*

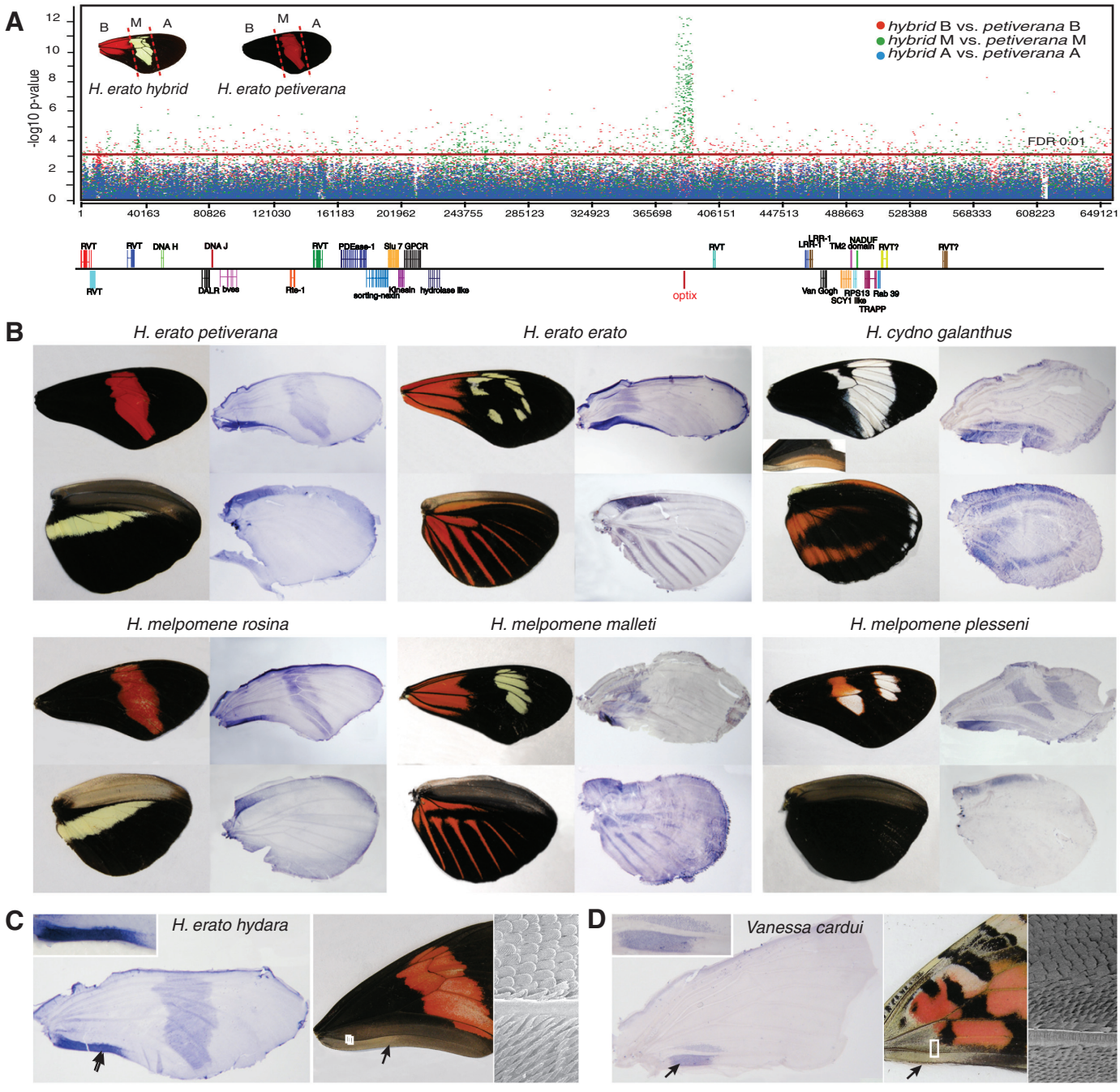

Fig. 2. *optix* expression prefigures red wing patterns in *Heliconius*. (**A**) *H. erato* genomic expression tiling microarrays spanning the entire red color pattern genomic map interval pinpoint *optix* as the only gene strongly differentially expressed in association with red forewing pattern elements. Details are provided in the SOM and fig. S1. (**B**) *optix* mRNA expression in 72-hour pupal wings of different species and races of *Heliconius* shows spatial association with all red wing patterns and (**C**) discrete patches of acute scales. (**D**) In *V. cardui*, *optix* expression is associated with acute scale patches but not color patterns.

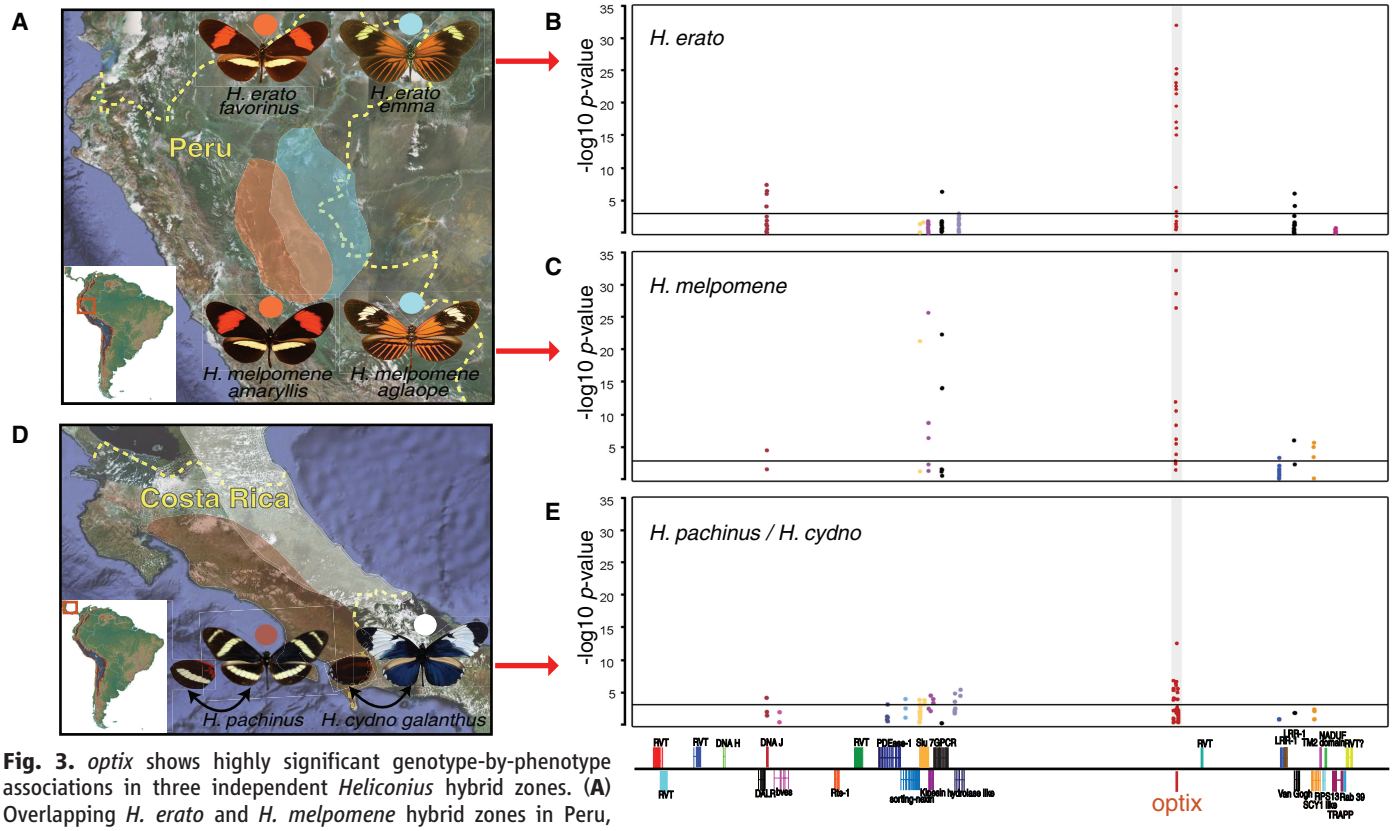

Fig. 3. *optix* shows highly significant genotype-by-phenotype associations in three independent *Heliconius* hybrid zones. (**A**) Overlapping *H. erato* and *H. melpomene* hybrid zones in Peru, where *optix* shows the strongest genotype-by-phenotype association across all the genes surveyed in (**B**) *H. erato* and (**C**) *H. melpomene.* (**D**) A Costa Rican *H. cydno*/*H. pachinus* hybrid zone where (**E**) *optix* shows the most significant genotype-by-phenotype association out of all the surveyed genes. The horizontal lines mark a false discovery rate of 0.001.

(fig. S2). None of these species showed color pattern–related expression of *optix*, even though both butterflies have red color patterns and *A. vanillae* is from a heliconiine genus closely related to *Heliconius*. In all lepidopteran species sampled, however, *optix* precisely prefigured small, discrete patches of specialized acute (pointed) scales (Fig. 2, C and D). We have identified several *H. melpomene* mutants that show homeotic transformations of normal red scales into acute scales (fig. S2), suggesting a simple regulatory switch between "red" and "acute" identities and demonstrating how *optix* might serve a dual function in determining these two scale types. In sum, our observations suggest that *optix* is ancestrally associated with acute scale morphology in lepidopteran pupal wings and that its color patterning function in *Heliconius* may be derived.

optix provides a compelling example of a gene that drives adaptation because its various alleles are regulatory variants that have pronounced effects on complex large-scale patterns. Because red color pattern variation is primarily achieved through *optix* cis-regulatory variation, we hypothesize that the different races within a given *Heliconius* species share a common wing prepattern that is interpreted by different *optix* alleles in different ways. Although the nature of this prepattern remains a mystery, the ability of *optix* to produce a complex variety of readouts from a common regulatory background suggests that it acts as a signal-integrating "input-output" regulatory gene (*11*). On the basis of this model, we speculate that *Heliconius* color pattern variation evolves primarily through the gain and loss of pattern-specific cis-regulatory elements, as do *Drosophila* wing melanin patterns (*12*, *13*), although we have yet to identify any specific *optix* cis-regulatory elements. That a single gene drives the evolution of both convergent and divergent color patterns across a range of species also presents a conceptual conundrum: Convergence and homology are often presented as contrasting explanations of similarity, yet the color patterns of comimetic *Heliconius* species could be considered both convergent and homologous under many modern definitions (*14*, *15*). The challenge now is to elucidate the functional role of *optix* in color pattern formation in order to understand how it was co-opted and why it served as such an efficient catalyst for the evolutionary radiation of *Heliconius* wing patterns.

References and Notes

1. J. Mallet, L. E. Gilbert, *Biol. J. Linn. Soc. London* **55**, 159 (1995).
2. K. S. J. Brown, thesis, Universidade Estadual de Campinas, Brazil (1979).
3. R. Papa, A. Martin, R. D. Reed, *Curr. Opin. Genet. Dev.* **18**, 559 (2008).
4. R. Papa *et al.*, *BMC Genomics* **9**, 345 (2008).
5. S. W. Baxter *et al.*, *Genetics* **180**, 1567 (2008).
6. N. L. Chamberlain, R. I. Hill, S. W. Baxter, C. D. Jiggins, M. R. Kronforst, *Heredity*, published online 9 February 2011 (10.1038/hdy.2011.3).
7. P. M. Sheppard, J. R. G. Turner, K. S. Brown, W. W. Benson, M. C. Singer, *Philos. Trans. R. Soc. London Ser. B* **308**, 433 (1985).
8. B. A. Counterman *et al.*, *PLoS Genet.* **6**, e1000796 (2010).
9. S. W. Baxter *et al.*, *PLoS Genet.* **6**, e1000794 (2010).
10. N. Pohl, M. P. Sison-Mangus, E. N. Yee, S. W. Liswi, A. D. Briscoe, *BMC Evol. Biol.* **9**, 99 (2009).
11. D. L. Stern, V. Orgogozo, *Science* **323**, 746 (2009).
12. B. Prud'homme *et al.*, *Nature* **440**, 1050 (2006).
13. T. Werner, S. Koshikawa, T. M. Williams, S. B. Carroll, *Nature* **464**, 1143 (2010).
14. J. Arendt, D. Reznick, *Trends Ecol. Evol.* **23**, 26 (2008).
15. G. P. Wagner, *Nat. Rev. Genet.* **8**, 473 (2007).

Acknowledgments: We thank M. A. Flores and A. Portugal for help rearing butterflies, M.-J. Sung for help with electron microscopy, J. Miller for help with microarray analysis, and J. Mallet for sharing samples. Supported by funding from NSF (R.D.R., W.O.M., M.R.K.), NIH (H.M.H., M.R.K.), and Centre National de la Recherche Scientifique–Guyane (B.A.C.) Sequences are available on GenBank (JN102349–JN102354). Microarray data are available on Gene Expression Omnibus (GSE30221). Permission to collect and export butterfly tissue was provided by the Peruvian Ministerio de Agricultura and Instituto Nacional De Recursos Naturales (004-2008-INRENA-IFFS-DCB and 011756-AG-INRENA); the French Guiana Ministere de L'Ecologie, de L'Energie, du Developpemet Durable et de la Mar (BIODAD-2010-0433); the Ecuadorian Ministerio del Ambiente Ecuadorian (013-09 IC-FAU-DNB/MA); and the Panamanian Autoridad Nacional del Ambiente

(SC/A-7-11). W.O.M., F.N, and R.D.R. designed experiments and conducted initial work. R.P. produced butterfly crosses and generated and analyzed the microarray data with H.M.H. A.M. generated in situ hybridization data. B.A.C., C.P.-D., C.D.J., N.L.C, and M.R.K. contributed nucleotide association data. R.C. and G.H. assisted with positional cloning. R.P., A.M., B.A.C., and R.D.R. prepared figures and R.D.R. wrote the manuscript with support from R.P., A.M., and W.O.M. The authors declare that they have no competing financial interests.

Supporting Online Material
www.sciencemag.org/cgi/content/full/science.1208227/DC1
Materials and Methods
Figs. S1 and S2
Tables S1 to S5
References

11 May 2011; accepted 5 July 2011
Published online 21 July 2011;
10.1126/science.1208227

Chaperonins Facilitate KNOTTED1 Cell-to-Cell Trafficking and Stem Cell Function

Xianfeng Morgan Xu, Jing Wang, Zhenyu Xuan,* Alexander Goldshmidt, Philippa G. M. Borrill,† Nisha Hariharan,‡ Jae Yean Kim,§ David Jackson‖

Cell-to-cell communication in plants includes the selective trafficking of transcription factors and other signals through plasmodesmata. The KNOTTED1 (KN1) homeobox (KNOX) family transcription factors, which use this pathway, are essential for stem cell establishment and/or maintenance. Here we show that KN1 trafficking requires the chaperonin complex, which belongs to a group of cytosolic chaperones that fold specific substrate proteins. Genetic and physical interaction data show a functional relevance for chaperonins in KNOX family-dependent stem cell maintenance. Furthermore, tissue-specific complementation assays indicate a mechanistic basis for chaperonin function during the posttranslocational refolding process. Our study shows that chaperonins are essential for the cell-to-cell trafficking of a subset of mobile transcription factors and demonstrates the importance of chaperonin-dependent protein trafficking for plant stem cell function.

Cell-to-cell communication plays critical roles in specifying cell fate and coordinating development in all multicellular organisms. One way in which plant cells communicate is by the selective trafficking of transcription factors and other signals through plasmodesmata (PD), channels that traverse the cell wall and connect neighboring cells (*1*–*5*). The KNOTTED1 (KN1) homeodomain transcription factor was the first plant protein found to traffic selectively through PD. Subsequent discoveries identified a growing array of mobile signaling factors, including transcriptional regulators and small RNAs (*3*, *4*, *6*–*8*). Despite our increasing recognition of the importance of this pathway for transmitting signals between cells, the molecular factors that contribute to selective trafficking are largely unknown. Here, we identify chaperonins as essential for the cell-to-cell trafficking of transcription factors and demonstrate that chaperonin-dependent protein trafficking is required for plant stem cell function.

Previously, we established a trichome rescue system in *Arabidopsis* to follow KN1 cell-to-cell trafficking in vivo (*9*). This system relies on the observation that maize *KN1* can functionally replace its *Arabidopsis* homolog *SHOOTMERISTEMLESS* (*STM*), and STM protein has also been shown to traffic (*9*, *10*). Trichomes are leaf hairs that develop from the epidermis, and require the cell-autonomous activity of a MYB transcription factor, GLABROUS1 (GL1) (*11*). In our system, trichome development is rescued in the *gl1* mutant by expressing a GL1

Cold Spring Harbor Laboratory, Cold Spring Harbor, NY 11724, USA.

*Present address: Department of Molecular and Cell Biology, Center for Systems Biology, University of Texas at Dallas, 800 West Campbell Road, Richardson, TX 75080, USA.
†Present address: John Innes Centre, Norwich Research Park, Norwich, Norfolk NR4 7UH, UK.
‡Present address: Department of Molecular and Cell Biology, University of California, Berkeley, CA 94720–3200, USA.
§Present address: Division of Applied Life Science (BK21/World Class University program), Plant Molecular Biology and Biotechnology Research Center, Gyeongsang National University, Jinju 660-701, Korea.
‖To whom correspondence should be addressed. E-mail: jacksond@cshl.edu

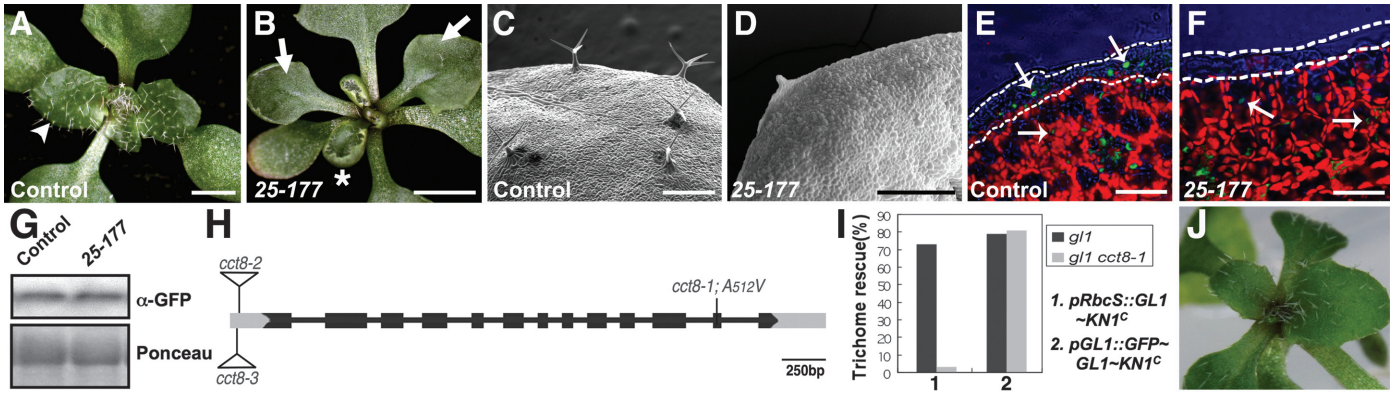

Fig. 1. Identification of a chaperonin, CCT8, essential for KN1 trafficking. (**A** and **B**) The starting line for mutagenesis (A) (*gl1; pRbcS::GFP~GL1~KN1*^{C}) showing trichome rescue (arrowhead), whereas the 25-277 mutant (B) lost trichome rescue (arrows) and had upwardly curled leaves (asterisk). (**C** and **D**) Scanning electron microscopic images of leaf epidermis from the starting line (C) or mutant (D). (**E** and **F**) Confocal image of a leaf cross section from the starting line (E) shows accumulation of GFP~GL1~KN1^C in both the mesophyll and the epidermis, whereas the 25-177 mutant (F) has normal accumulation of GFP~GL1~KN1^C in the mesophyll but a severe reduction in the epidermis. Dashed lines denote the epidermis; arrows point to nuclei with fusion protein. Chlorophyll autofluorescence is shown in red. Corresponding genotypes are marked in each image. (**G**) Western blotting shows a similar expression of the *pRbcS::GFP~GL1~KN1*^{C} transgene in both the starting line (control) and the 25-177 mutant. Ponceau staining was used as the loading control. (**H**) *CCT8* gene structure, showing different mutant alleles. Black bars indicate exons; lines and gray bars represent introns and untranslated regions, respectively. T-DNA insertions are shown as open triangles. (**I**) Control experiments: (1) Mesophyll-expressed GL1~KN1^C could rescue trichomes in *gl1* but failed to rescue in *gl1; cct8-1*. (2) Expression of the GFP~GL1~KN1^C fusion in the *gl1; cct8-1* epidermis was sufficient to rescue trichomes. Trichome rescue efficiency was scored as the percentage of T1 transformants ($n > 40$) with trichome rescue. (**J**) A *pfd6-1; gl1; pRbcS::GFP~GL1~KN1*^{C} plant showing normal trichome rescue. Scale bars: 0.5 cm (A and B), 400 μm (C and D), 25 μm (E and F).